Position Control of Soft Manipulators with Dynamic and Kinematic Uncertainties

E. Franco*, J. Tang**, A. Garriga Casanovas*, F. Rodriguez y Baena*, A. Astolfi**

**Mechanical Engineering Department, Imperial College London, SW7 2AZ, London, UK
(e-mail: e.franco11@imperial.ac.uk, a.garriga-casanovas14@imperial.ac.uk, f.rodriguez@imperial.ac.uk).
** Department of Electrical and Electronic Engineering Imperial College London, (e-mail: jacky.tang18@imperial.ac.uk)
***Department of Electrical and Electronic Engineering, Imperial College London, SW7 2AZ, London, UK and Dipartimento
di Ingegneria Civile e Ingegneria Informatica, Università di Roma "Tor Vergata", Via del Politecnico 1, 00133 Roma, Italy
(e-mail: a.astolfi@imperial.ac.uk)*

Abstract: This work investigates the position control problem for a soft continuum manipulator in Cartesian space intended for minimally invasive surgery. Soft continuum manipulators have a large number of degrees-of-freedom and are particularly susceptible to external forces because of their compliance. This, in conjunction with the limited number of sensors typically available, results in uncertain kinematics, which further complicates the control problem. We have designed a partial state feedback that compensates the effects of external forces employing a rigid-link model and a port-Hamiltonian approach and we have investigated in detail the use of integral action to achieve position regulation in Cartesian space. Local stability conditions are discussed with a Lyapunov approach. The performance of the controller is compared with that achieved with a radial-basis-functions neural network by means of simulations and experiments on two prototypes.

Keywords: Disturbance Rejection, Lagrangian and Hamiltonian systems, Passivity-based control.

1. INTRODUCTION

Soft robots have desirable features for minimally invasive surgery (MIS) such as light weight, high deformability and adaptability to the environment. Soft robotic manipulators for MIS are characterized by slender bodies that allow access to natural orifices or small incisions, in a similar fashion to conventional endoscopes (Runciman, Darzi, & Mylonas, 2019). Additionally, their structural compliance could reduce the risk of damaging internal organs as a result of accidental movements or of deformations of the tissues. Nevertheless, several challenges remain before soft robots can be extensively used in clinical practice. These include the ability to exert sufficient forces with miniaturized actuators, and to achieve reliable and accurate positioning (Thuruthel, Ansari, Falotico, & Laschi, 2018). Common actuation principles for soft continuum manipulators include pneumatics, cable driven, hydraulics, and shape memory alloy. Among pneumatic systems, the flexible micro actuator (FMA), originally proposed in (Suzumori, 1996), has inspired a variety of designs, including our recent work (Garriga-Casanovas, Collison, & Rodriguez y Baena, 2018). FMAs have internal chambers that can be pressurized independently resulting in bending of the actuator on different planes. Since FMAs and soft continuous manipulators in general, have a large number of degrees-of-freedom (DOFs), their configuration is typically reconstructed from a limited number of sensors. In the absence of external forces, FMAs bend with constant curvature (CC), thus their tip position in the Cartesian space is uniquely defined by the bending angle. Disturbances, which are ubiquitous in MIS applications, invalidate the CC assumptions resulting in uncertain

kinematics. Data-driven and numerical approaches for kinematic model identification and kinematic based control of soft continuum manipulators include: Kalman filters (Li, Kang, Branson, & Dai, 2018); machine learning techniques (Thuruthel et al., 2017); reduced-order finite element methods (Bieze et al., 2018). Analytical approaches can be divided into those based on continuum models, such as Cosserat beam theory (Renda, Boyer, Dias, & Seneviratne, 2018); discrete parameter models, such as piecewise constant curvature (PCC) (Katzschmann, Santina, Toshimitsu, Bicchi, & Rus, 2019); and rigid-link models (Godage, Wirz, Walker, & Webster, 2015). While continuum models are more accurate, they do not typically allow for closed-form solutions. Instead, discrete models are more computationally efficient, but introduce approximations that should be accounted for in the system dynamics. In summary, soft continuum manipulators combine the difficulties of uncertain dynamics and those of uncertain kinematics, posing a remarkable challenge from a control prospective.

A variety of control approaches have been proposed for this class of systems, including feedback linearization (Falkenhahn, Hildebrandt, Neumann, & Sawodny, 2017), sliding mode control (Alqumsan, Khoo, & Norton, 2019), and passivity based control (Mattioni, Wu, Ramirez, Gorrec, & Macchelli, 2018). However, feedback linearization is sensitive to model uncertainties, while sliding mode control employs high gains which can alter the system compliance in closed loop. We have recently developed an adaptive partial-state feedback control based on the Interconnection and Damping Assignment Passivity based control methodology (IDA-PBC) (Ortega, Spong, Gomez-Estern, & Blankenstein,

2002) that compensates the effect of external disturbances in FMAs (Franco et al., 2019; Franco & Garriga-Casanovas, 2020). The extension of these ideas to position regulation in Cartesian space is not straightforward because of kinematic uncertainties. In this work we introduce an integral action to regulate the position of our manipulators in Cartesian space. Local stability conditions are analyzed with a Lyapunov approach. The performance of the controller is then compared with that achieved with a different estimator based on a radial-basis-functions neural network via simulations and experiments on two soft continuum prototypes.

Section 2 describes the system model and gives an overview of the IDA-PBC methodology. Section 3 details the controller design. Section 4 presents simulations and experimental results. Section 5 contains concluding remarks.

2. PROBLEM FORMULATION

2.1 System overview

The soft continuum manipulators considered in this work have three internal chambers spaced at $2\pi/3$ and an inextensible thread running along their central axis to prevent elongation, see (Garriga-Casanovas et al., 2018). A second thread is wound around the external surface of the manipulators to prevent radial expansion. The structural stiffness k of the manipulators is assumed constant and uniform. The internal pressures P_1, P_2, P_3 produce a bending moment resulting in the tip rotation θ on the bending plane. The orientation of the bending plane with respect to a fixed reference frame is defined by the angle φ. The angles θ and φ depend on P_1, P_2, P_3 according to (Suzumori, 1996)

$$\theta = \frac{1}{k\sqrt{2}}\sqrt{(P_1 - P_2)^2 + (P_1 - P_3)^2 + (P_3 - P_2)^2}$$
$$\tan(\varphi) = \frac{\sqrt{3}(P_1 - P_2)}{P_1 + P_2 - 2P_3}. \tag{1}$$

The manipulator is modelled as a rigid-link system (Godage et al., 2015) consisting of n virtual elastic joints in the plane of bending (see Figure 1). The control input is thus defined as $u = \sqrt{(P_1 - P_2)^2 + (P_1 - P_3)^2 + (P_3 - P_2)^2}$ (see Figure 2). The system dynamics on the bending plane can be described in port-Hamiltonian form as

$$\begin{bmatrix} \dot{q} \\ \dot{p} \end{bmatrix} = \begin{bmatrix} 0 & I \\ -I & -R \end{bmatrix} \begin{bmatrix} \nabla_q H \\ \nabla_p H \end{bmatrix} + \begin{bmatrix} 0 \\ G \end{bmatrix} u - \begin{bmatrix} 0 \\ \delta \end{bmatrix}, \tag{2}$$

where $H = \frac{1}{2}p^T M^{-1}p + V$ is the Hamiltonian, with potential energy V and inertia matrix $M(q) = M^T$. The system states are the virtual positions $q(t) \in \mathbb{R}^n$ and the momenta $p = M\dot{q}$. The constant matrix G is a column vector, thus rank$\{G\} = 1$ which indicates underactuation. The effects of external forces and of model uncertainties are lumped in the disturbance δ which includes matched components (i.e. those affecting the actuated DOF) and unmatched components (i.e. those affecting the unactuated DOF). The damping matrix is $R > 0$, while I is the identity matrix.

2.2 Overview of IDA-PBC design

The design approach is based on the IDA-PBC methodology (Ortega et al., 2002) and achieves the closed-loop dynamics

$$\begin{bmatrix} \dot{q} \\ \dot{p} \end{bmatrix} = \begin{bmatrix} 0 & M^{-1}M_d \\ -M_d M^{-1} & J_2 - RM^{-1}M_d - Gk_v G^T \end{bmatrix} \begin{bmatrix} \nabla_q W \\ \nabla_p W \end{bmatrix}, \tag{3}$$

with storage function $W = H_d + \Lambda^T(q - q^*) + C$, where $H_d = \frac{1}{2}p^T M_d^{-1}p + V_d$ is the desired Hamiltonian. The controller parameters are the inertia matrix M_d, the potential energy V_d, and the free matrix $J_2 = -J_2^T$, which should satisfy the partial differential equations (PDEs)

$$G^\perp\left(\nabla_q V - M_d M^{-1}\nabla_q V_d\right) = 0 \tag{4.a}$$

$$G^\perp\left(\nabla_q(p^T M^{-1}p) - M_d M^{-1}\nabla_q(p^T M_d^{-1}p) + 2J_2 M_d^{-1}p\right) = 0 \tag{4.b}$$

where $G^\perp$ is such that $G^\perp G = 0$ and rank$(G^\perp) = n - 1$. The term Λ can be interpreted as a vector of closed-loop non-conservative forces and should verify the algebraic equations

$$G^\perp(\delta - M_d M^{-1}\Lambda) = 0. \tag{5}$$

If δ is constant and known and if q is bounded, then $W > 0$ and the control law that achieves (3) is as in (Franco, 2019a)

$$u = u_{es} + u_{di} + u^*,$$
$$u_{es} = G^\dagger\left(\nabla_q H - M_d M^{-1}\nabla_q H_d + J_2\nabla_p H_d\right),$$
$$u_{di} = -k_v G^T\nabla_p H_d,$$
$$u^* = G^\dagger(\delta - M_d M^{-1}\Lambda), \tag{6}$$

where $G^\dagger = (G^T G)^{-1}G^T$. Instead, state dependent disturbances, which are part of our future work, can be accounted for as in (Franco, 2019b; Franco, Rodriguez Y Baena, & Astolfi, 2020). For simplicity, the effect of the weight of the manipulator is not accounted for in the potential energy $V = q^T kq/2$, and the damping matrix is assumed diagonal and constant. The effects of these approximations are included in the lumped disturbance δ. Since $G = [1_n]$ is constant, the tip rotation is $G^T q = \theta$. Setting $M_d = k_m M$ and $J_2 = 0$ solves (4.b), while (4.a) yields

$$V_d = \frac{k}{2k_m}\sum_{i=1}^n q_i^2 - \frac{k}{2nk_m}\theta^2 + \frac{k_p}{2k_m}(\theta - \theta^*)^2, \tag{7}$$

which has a strict minimizer in $\theta = \theta^*$. The domain of attraction can be approximated as $\Omega = \{q \in \mathbb{R}^n | V_d < c\}$. Substituting (7) in (6) yields the control law (Franco & Garriga-Casanovas, 2020)

$$u = \frac{k}{n}\theta - k_p(\theta - \theta^*) - \frac{k_v}{k_m}\dot{\theta} + G^\dagger(\hat{\delta} - k_m\Lambda), \tag{8}$$

where k_p, k_m, k_v are positive tuning parameters, and $\hat{\delta}$ is an estimate of δ. In particular, solving (5) with

$$\Lambda_i = \frac{1}{nk_m}\left((n-1)\delta_i - \sum_{j=1}^n \delta_{j\neq i}\right) \tag{9}$$

results in $G^\dagger\Lambda = 0$, thus this term does not appear in (8). The disturbances are estimated adaptively from (2) with a variation of the *Immersion and Invariance* method (Astolfi, Karagiannis, & Ortega, 2007), giving the dynamic estimator

$$\dot{\hat{\delta}} = -\alpha(\nabla_q V + R\dot{q} - Gu + \hat{\delta}). \qquad (10)$$

Pre-multiplying (10) by the constant matrix $G^\dagger$ results in

$$G^\dagger \dot{\hat{\delta}} = -\alpha\left(\frac{k\theta}{n} + \frac{R\dot{\theta}}{n} - u + G^\dagger \hat{\delta}\right), \qquad (11)$$

which only depends on the tip rotation θ and on its first order time derivative. As a result, controller (8) is implementable and achieves the regulation goal $\theta = \theta^*$ in the presence of constant disturbances (Franco & Garriga-Casanovas, 2020).

Regulating the tip position of the manipulator in Cartesian space is however not immediate since the mapping $(x, y) = f(q)$ is not known. Even though (8) is a linear control law, simply replacing θ with x would alter the closed-loop dynamics since the relationship between these two variables is nonlinear. Additionally, the physical interpretation of the control in terms of energy shaping would be lost since the potential energy is not directly related to the position (x, y).
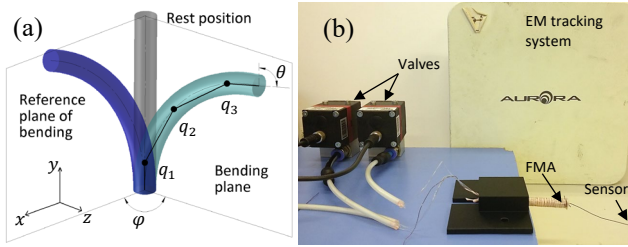

Fig. 1. Schematic of the rigid-link model showing different configurations (a); test setup with one FMA (b).

3. MAIN RESULT

The control aim considered in this work is the regulation of the tip position in Cartesian space. This is achieved combining controller (8) and the adaptive law (11) with an integral action that estimates the mapping $(x, y) = f(q)$. For illustrative purposes, we consider the regulation goal $x = x^*$ on the bending plane.

Lemma 1: Given the mapping $x = f(\theta)$, assume that there exist a function σ and some positive values σ_0 and σ_1 such that $x^* - x = \sigma(\theta^* - \theta)$ with $\sigma > \sigma_0$, and that $|\dot{\sigma}|/\sigma^2 < \sigma_1$. Consider the observer state $\hat{\theta}$ with the update law

$$\dot{\hat{\theta}} = k_I(x^* - x). \qquad (12)$$

Then $\hat{\theta}$ converges exponentially to θ^*, where $x^* = f(\theta^*)$, for all $k_I > \sigma_1$.

Proof: Define the observer error $\varsigma = \theta^* - \hat{\theta}$. By hypothesis there exist some function $\sigma > \sigma_0 > 0$ for which $x^* - x = f(\theta^*) - f(\hat{\theta}) = \sigma\varsigma$ (e.g. the hypothesis is verified for a continuously differentiable and monotonically increasing mapping f). Defining the storage function $W_0 = \frac{1}{2}(x^* - x)^2 = \frac{1}{2}\sigma^2\varsigma^2$ and computing its time derivative along the system's trajectories yields

$$\dot{W}_0 = \sigma^2\varsigma\dot{\varsigma} + \sigma\dot{\sigma}\varsigma^2. \qquad (13)$$

Observing that $\dot{\varsigma} = -\dot{\hat{\theta}}$ and substituting (12) yields

$$\dot{W}_0 = \varsigma\dot{\varsigma} = -(k_I\sigma^2 - \dot{\sigma})\sigma\varsigma^2. \qquad (14)$$

Then $\dot{W}_0 < 0$ for all $k_I > \sigma_1 > |\dot{\sigma}|/\sigma^2$ and ς converges to zero exponentially, concluding the proof ∎

For our prototypes, the maximum tip rotation is bounded so that $|\theta| < \pi/2$. While larger rotations are theoretically possible employing larger pressures, in practice this results in leakages from the internal chambers thus $|\theta|$ does not increase further. In the present case the mapping $x = f(\theta)$ is a trigonometric function and it is monotonically increasing provided that the measurement frame and the robot frame are chosen so that x and θ have the same sign.

Proposition 1: Consider system (2) with the mapping $x = f(\theta)$ in closed loop with the control law

$$u = \frac{k}{n}\theta - k_p(\theta - \hat{\theta}) - \frac{k_v}{k_m}\dot{\theta} + G^\dagger\delta, \qquad (15)$$

where $G^\dagger\dot{\hat{\delta}}$ is given in (11) and $\hat{\theta}$ is given in (12). Assume that there exist positive constants σ_0 and σ_1 such that $\sigma > \sigma_0$ and $|\dot{\sigma}|/\sigma^2 < \sigma_1$ for all θ, and that $|\delta|$ is bounded from above. Then there exist values of R, α, k_m, k_v, and k_I such that the equilibrium $x = x^*$ is locally stable and x converges to x^* asymptotically for all $k_p > 0$.

Proof: Defining the disturbance estimation error $z = \hat{\delta} - \alpha p - \delta$ as in (Franco et al., 2019) and substituting (15) in (2) yields

$$\dot{p} = -k_m\nabla_q W - (Rk_m + Gk_v G^T)\nabla_p W + k_p G\varsigma + \alpha p + z. \quad (16)$$

Defining the Lyapunov function candidate

$$W' = W + W_0 + z^T z/2, \qquad (17)$$

computing its time derivative along the trajectories of the system and substituting (11), (12), and (16) yields

$$\dot{W}' = -R\dot{q}^2/k_m - k_v\dot{\theta}^2/k_m^2 + \dot{q}^T(z + \alpha p + k_p G\varsigma)/k_m$$
$$-(k_I\sigma^2 - \dot{\sigma})\sigma\varsigma^2 - \alpha z^T(z - \nabla_q(p^T M^{-1}p) + \alpha p) \quad (18)$$
$$+ \dot{\Lambda}^T(q - q^*) - z^T\dot{\delta}.$$

Since the elements of M depend on the cosine of the virtual positions q_i, we have that $\max\{M\} < m_T$, with m_T the mass of the manipulator and $\max\{M\}$ the largest element of M. Thus the inequalities $|p| \le c_1 m_T|\dot{q}|$ and $\nabla_q(p^T M^{-1}p)/2 \le c_2 m_T|\dot{q}|^2$ hold for some $c_1 > 0$ and $c_2 > 0$. Additionally, using the Young's inequalities $|z^T\dot{\delta}| \le |\dot{\delta}|^2 + |z|^2/4$ and $|z^T||\dot{q}^2| \le |\dot{q}|^4 + |z|^2/4$ and rearranging terms in (18) yields

$$\dot{W}' \le -[\dot{\theta} \quad \varsigma]\begin{bmatrix} k_v/2k_m^2 & \star \\ -k_p/2k_m & (k_I\sigma^2 - \dot{\sigma})\sigma \end{bmatrix}\begin{bmatrix} \dot{\theta} \\ \varsigma \end{bmatrix}$$
$$-[\dot{q}^T \quad z^T]\begin{bmatrix} (R - \alpha c_1 m_T)/k_m & \star \\ \frac{1}{2}(\alpha^2 c_1 m_T - 1/k_m) & \alpha - \frac{(\alpha^2 + 1)}{4} \end{bmatrix}\begin{bmatrix} \dot{q} \\ z \end{bmatrix} \quad (19)$$
$$-k_v\dot{\theta}^2/2k_m^2 + |\dot{\delta}|^2 + c_2^2 m_T^2|\dot{q}|^4 + \dot{\Lambda}^T(q - q^*).$$

Employing a Schur complement argument we conclude that $\dot{W}' \le 0$ provided that $\alpha, k_p, k_m, k_v, k_I$ are such that

$$(R - \alpha c_1 m_T)(4\alpha - 1 - \alpha^2) > k_m(\alpha^2 c_1 m_T - 1/k_m)^2$$
$$k_v(k_I \sigma^2 - \dot{\sigma})\sigma > k_p^2 /2 \tag{20}$$
$$k_v \dot{\theta}^2 > 2k_m^2 \left(\left| \dot{\delta} \right|^2 + c_2^2 m_T^2 |\dot{q}|^4 + \dot{\Lambda}^T(q - q^*) \right).$$

It follows from (19) that $\dot{q}, \dot{\theta}, z, \varsigma \in \mathcal{L}_2 \cap \mathcal{L}_\infty$. Additionally, it follows from (16) that $\dot{p} \in \mathcal{L}_\infty$ and thus $\ddot{q} \in \mathcal{L}_\infty$. Computing the time derivative of z and substituting (10) and (16) yields

$$\dot{z} = -\alpha(z - \nabla_q(p^T M^{-1} p) + \alpha p) + \dot{\delta}. \tag{21}$$

Since $\dot{\delta}$ is bounded by hypothesis, then $\dot{z} \in \mathcal{L}_\infty$. Thus, according to Barbalat's Lemma, $\dot{p}, \dot{\theta}, z, \varsigma$ converge to zero asymptotically. Substituting $\dot{p} = \dot{\theta} = z = \varsigma = 0$ in (16) yields $\nabla_q W = 0$ or equivalently $\nabla_q V_d + \Lambda = 0$. Substituting (7) and (9) in the former equation and pre-multiplying by $G^\dagger$, while recalling that $G^\dagger \Lambda = 0$, gives

$$G^\dagger \nabla_q V_d + G^\dagger \Lambda = (\theta - \hat{\theta}) k_p / k_m. \tag{22}$$

Thus θ converges to $\hat{\theta}$ asymptotically. Since $\sigma < \sigma_0$ and since $|\dot{\sigma}|/\sigma^2 < \sigma_1$ by hypothesis, there exist some R, α, k_v, k_m, k_I that verify inequalities (20). Finally, it follows from *Lemma 1* that $\hat{\theta}$ converges to θ^* concluding the proof ■

Since FMAs typically have a small mass (i.e. $m_T \ll 1$), the inequalities (20) can be simplified omitting terms in m_T as

$$\alpha^2 - 4\alpha + 1 + 1/(k_m R) < 0$$
$$k_I > k_p^2 /(2k_v \sigma^3) + |\dot{\sigma}|/\sigma^2 \tag{23}$$
$$k_v \dot{\theta}^2 > 2k_m^2 |\dot{\delta}|^2 + 2k_m^2 |\dot{\Lambda}||q - q^*|,$$

which represent sufficient stability conditions. The first inequality in (23) is verified by the following set of values $2 - \sqrt{3 - 1/(k_m R)} < \alpha < 2 + \sqrt{3 - 1/(k_m R)}$, provided that $k_m R > 1/3$. This indicates that either a sufficiently large damping R or a large k_m are required to ensure stability of the equilibrium. However, increasing k_m affects the third inequality, which demands a larger k_v. The latter can result in a slower transient, which might not be desirable for some applications. It follows from (9) that $|\dot{\Lambda}| < |\dot{\delta}|$ if $k_m > 1$ and, since the tip rotation is limited by $|\theta| < \pi/2$, the third inequality can be further simplified as $k_v \dot{\theta}^2 > 2k_m^2 |\dot{\delta}|(|\dot{\delta}| + \pi/2)$. The second inequality expresses a more stringent condition on k_I compared to *Lemma 1*. For $n = 1$ we have $x = \sin(\theta)$ thus, employing Taylor series, $\sigma = (1 - \theta^2/6)$. Hence $\sigma > 1/2$ for all $|\theta| < \pi/2$, while $\dot{\sigma} = -\theta\dot{\theta}/3$ is bounded as a result of *Proposition 1*. Thus, the second inequality in (23) is verified by $k_I \geq 4k_p^2/k_v + 4|\dot{\sigma}|$.

The result of *Proposition 1* can be readily extended to the regulation of the three coordinates (x, y, z) of the tip of a manipulator consisting of multiple FMAs. Since each FMA has one actuated DOF on the plane of bending, two FMAs connected in series are required to regulate simultaneously the two coordinates (x, y) of the tip of the manipulator (see Figure 2). The control input for each FMA is then computed using (15) and (11) replacing θ with θ_1, θ_2, which are kinematically decoupled and represent the tip rotations of each FMA with respect to its base. Two separate observers

(12) should then be employed to estimate the mappings $x = f(\theta_1)$ and $y = f(\theta_2)$. Varying the individual pressures in the internal chambers of the first FMA while preserving u_1, results in different orientations φ_1 of the bending plane according to (1). This additional DOF allows regulating the remaining coordinate z by using a third separate observer that estimates the mapping $z = f(\varphi_1)$. This result is summarized in the following corollary, omitting the proof for brevity.

Corollary 1: Consider system (2) consisting of two FMAs connected in series, each approximated with a n DOF rigid-link model, in closed-loop with the control laws

$$u_j = \frac{k}{n}\theta - k_p(\theta_j - \hat{\theta}_j) - \frac{k_v}{k_m}\dot{\theta}_j + \tilde{\delta}_j,$$
$$\dot{\tilde{\delta}}_j = \alpha\left(\frac{k\theta_j}{n} + \frac{R\dot{\theta}_j}{n} - u_j + \tilde{\delta}_j\right), \tag{24}$$

where $1 \leq j \leq 2$ and $\hat{\theta}_1(x), \hat{\theta}_2(y), \hat{\varphi}_1(z)$ are each estimated independently with the integral action (12), and $\hat{\varphi}_1$ depends on the internal pressures P_1, P_2, P_3 according to (1). Then the equilibrium position associated to the coordinates $(x, y, z) = (x^*, y^*, z^*)$ within the reachable workspace of the manipulator is locally stable and the tip position (x, y, z) converges to (x^*, y^*, z^*) asymptotically provided that R, α, k_m, k_v, k_I satisfy the inequalities (20) for all j.

The peripheral FMA, due to its weight, introduces an additional disturbance on the first one. This results in kinematic and dynamic coupling between the two FMAs, which is accounted for by the scalar values of the lumped disturbances $\tilde{\delta}_j$. Notably, the regulation of the z coordinate only depends on the observer $\dot{\hat{\varphi}}_1 = k_I(z^* - z)$, since the relationship between the internal pressures and the orientation of the bending plane is purely geometrical (see Figure 2).
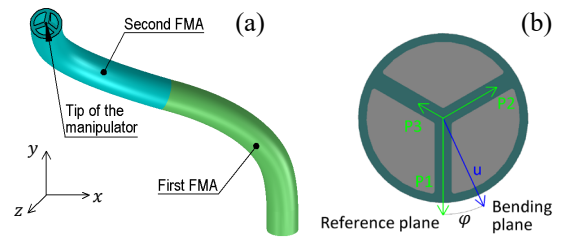

Fig. 2. Schematic of a soft manipulator consisting of two FMAs connected in series (a); section view of one FMA (b): the control input u is the vector sum of the internal pressures which define the bending plane and the tip rotation.

Adding a third FMA in series allows regulating all 6 DOFs at the tip of the manipulator. In practice, the position regulation is only possible within the reachable workspace of the manipulator, which depends on the dimension and number of FMAs, but also on the disturbances. A computation of the reachable workspace should thus be performed at each instant based on the current state and on the estimated disturbances. The study of this aspect is part of our future work.

4. EXPERIMENTAL RESULTS

4.1 Simulations

The model (2) and the control law (24) with the integral observer (12) have been simulated in Matlab using the parameters $k = 5$, $R = 0.1$, $m_T = 1.5$, $n = 3$, $k_p = 0.2$, $k_m = 10$, $k_v = 10$, $\alpha = 1$, and $k_I = 5$, which verify inequalities (23) for all $\sigma > 0.3$ and $\dot{\delta}^2 < 0.03\dot{\theta}^2$. For comparison purposes, a different approach based on a radial-basis-functions neural network (RBFNN) has been employed to estimate the mapping $x = f(\theta)$. The RBFNN has a simple structure consisting of three layers (i.e. input layer, hidden layer, and output layer) and can approximate highly nonlinear functions (Park & Sandberg, 1991). The hidden layer consists of $m = 2$ neurons implemented with a Gaussian function

$$\phi_j(x) = \exp\left(\frac{\|x - c_j\|}{2\rho_j^2}\right),$$

where c_j is the center and ρ_j is the width of the neuron j. The output of the RBFNN estimator is then computed as

$$\hat{\theta} = W\Phi,$$

where Φ is the vector of the elements ϕ_j. The term W is a scalar matrix of weights computed from training data, which consist of known pairs (x, θ). The latter pairs are gathered recursively at run time in batches of size b, where b_0 is the initial batch size. In summary, the parameters of the RBFNN estimator are c_j, ρ_j, b, b_0 and m, which have been set as $c_j = 0, \rho_j = 1, b = 100, b_0 = 5000, m = 2$ in simulations. These values are the result of an extensive parameter search.
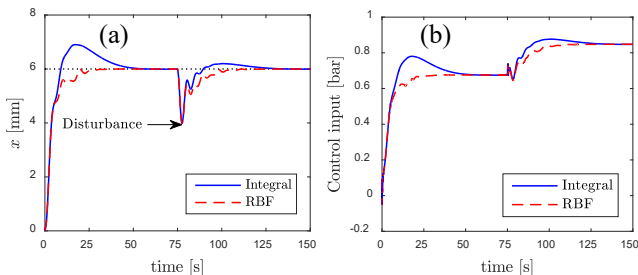

Fig. 3. Simulation results with disturbance acting at 75 seconds: (a) tip position x; (b) corresponding control input.

For illustrative purposes, the regulation of the tip position along the x axis for one FMA in the presence of an impulsive disturbance (i.e. a lateral force $F = 0.01\ N$ acting on the tip at time $t = 75$ seconds) is shown in Figure 3. The observer (12) results in a smoother response and a slower convergence to the equilibrium position compared to that obtained with the RBFNN estimator. Employing larger values of k_I results in faster response but also increases the initial overshoot. This issue could be addressed with anti-windup strategies, which will be investigated as part of our future work.

4.2 Experiments

The controller (24) has been tested with two soft continuum prototypes that employ pneumatic actuation (Garriga-Casanovas et al., 2018). The first test setup is shown in Figure 1 and employs proportional pressure regulators (Tecno Basic, Hoerbiger, Germany) supplying the internal chambers of one FMA, and an electromagnetic tracking system (NDI

Aurora, Canada) measuring the position and orientation of the tip of the manipulator. The mass of one FMA is $m_T = 1.5$ grams and the damping matrix has been estimated experimentally as $R = \text{diag}\{0.03\}$. The controller parameters have been set as $k_p = 0.2, k_m = 20, k_v = 1, \alpha = 1, k_I = 10$ and $n = 3$ for (24) with the observer (12), which verify inequalities (23) for all $\sigma > 0.2$ and for all $\dot{\delta}^2 < 0.01\dot{\theta}^2$. To obtain a comparable response with both estimation methods, the parameters of the RBFNN estimator have been set as $c = 0, \rho = 1, b_0 = 75, b = 75$, and $m = 2$ neurons.
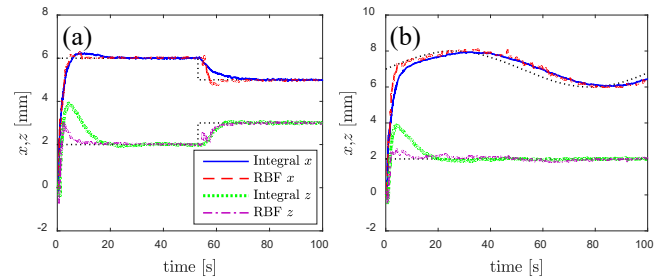

Fig. 4. Experimental results for one FMA: (a) tip coordinates x and z for constant setpoint; (b) tip coordinates x and z for continuously varying setpoint (i.e. sinusoidal path on x).
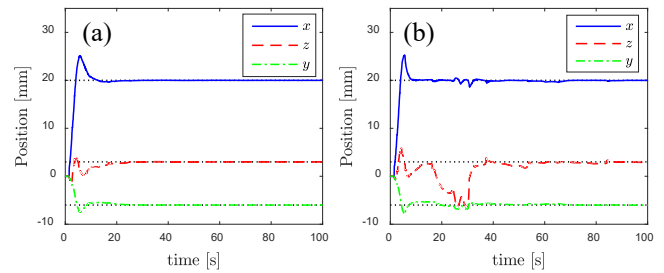

Fig. 5. Experimental results for two FMA: (a) tip coordinates x, y and z with integral observer (12); (b) tip coordinates x, y and z with RBFNN estimator.

The regulation of the tip position along the x and z axes for one FMA is illustrated in Figure 4. The controller (24) correctly compensates the disturbances, which are due to the weight of the manipulator and of the sensor, and the model uncertainties. The observer (12) and the RBFNN estimator have been employed to regulate the coordinates $(x, z) = (x^*, z^*)$ in the case of a constant setpoint and of a sinusoidal path. In both cases the experimental results show a good agreement with the simulations. The closed-loop response is faster than in simulation because of the larger value of k_m used, which effectively scales down the derivative gain k_v in (24). The regulation of all three coordinates (x, y, z), is achieved with two FMAs connected in series (Figure 5). In this setup the weight of the distal FMA acts as an additional disturbance on the first FMA. Notably, the RBFNN estimator with the same tuning parameters results in a more oscillatory response, which appears erratic on the z axis. This could be due to the larger disturbances acting on the first FMA, which includes out-of-plane components. This behavior could also highlight a limitation of our implementation, which employs separate RBFNN estimators for each coordinate. A detailed investigation of this aspect is part of our future work.

In summary, the tip position of the manipulator in Cartesian space can be regulated with either the RBFNN estimator or the observer (12) combined with the controller (24). The simulations and the experimental results suggest that the RBFNN estimator can lead to a faster response, depending on the tuning parameters employed. Conversely, the integral observer (12) results in a smoother but slower response. Notably, the integral observer (12) introduces only one additional parameter, while the RBFNN estimator requires tuning four parameters. Additionally, *Proposition 1* ensures local stability of the desired equilibrium provided that the inequalities (20) are verified. Instead, no equivalent stability conditions could be derived for the RBFNN estimator.

6. CONCLUSIONS

This paper has investigated the position regulation problem for a class of soft continuum manipulators similar to FMA in Cartesian space. To this end we have added an integral action to a partial-state feedback control with adaptive disturbance compensation. Sufficient conditions for the stability of the desired equilibrium have been expressed highlighting the effect of the tuning parameters. The performance of the controller has been assessed via simulations and via experiments on two soft continuum prototypes. The comparison with a RBFNN estimator suggests that the integral action results in a slower but smoother response over a range of setpoints and of external disturbances. The RBFNN estimator leads to a faster convergence to the equilibrium position, but can result in overshoot, oscillations, and even erratic behavior in the case of larger disturbances.

ACKNOWLEDGEMENTS

REFERENCES

Alqumsan, A. A., Khoo, S., & Norton, M. (2019). Robust control of continuum robots using Cosserat rod theory. *Mechanism and Machine Theory*, 131, 48–61.

Astolfi, A., Karagiannis, D., & Ortega, R. (2007). *Nonlinear and Adaptive Control with Applications*. (Springer-Verlag).

Bieze, T. M., Largilliere, F., Kruszewski, A., Zhang, Z., Merzouki, R., & Duriez, C. (2018). Finite Element Method-Based Kinematics and Closed-Loop Control of Soft, Continuum Manipulators. *Soft Robotics*, 5(3), 348–364.

Falkenhahn, V., Hildebrandt, A., Neumann, R., & Sawodny, O. (2017). Dynamic Control of the Bionic Handling Assistant. *IEEE/ASME Transactions on Mechatronics*, 22(1), 6–17.

Franco, E. (2019a). Adaptive IDA-PBC for underactuated mechanical systems with constant disturbances. *International Journal of Adaptive Control and Signal Processing*, 33(1), 1–15.

Franco, E. (2019b). IDA-PBC with Adaptive Friction Compensation for Underactuated Mechanical Systems. *International Journal of Control*, 1–29.

Franco, E., Garriga-Casanovas, A., Rodriguez y Baena, F., & Astolfi, A. (2019). Model based adaptive control for a soft robotic manipulator. *2019 IEEE Conference on Decision and Control*, 1019-1024.

Franco, E., & Garriga-Casanovas, A. (2020). Energy Shaping Control of Soft Continuum Manipulators with in-plane Disturbances. *The International Journal of Robotics Research*, OlineFirst, 1-20.

Franco, E., Rodriguez Y Baena, F., & Astolfi, A. (2020). Robust Dynamic State Feedback for Underactuated Systems with Linearly Parameterized Disturbances. *International Journal of Robust and Nonlinear Control*, 1–17.

Garriga-Casanovas, A., Collison, I., & Baena, F. R. y. (2018). Toward a Common Framework for the Design of Soft Robotic Manipulators with Fluidic Actuation. *Soft Robotics*, 5(5), 622–649.

Godage, I. S., Wirz, R., Walker, I. D., & Webster, R. J. (2015). Accurate and Efficient Dynamics for Variable-Length Continuum Arms: A Center of Gravity Approach. *Soft Robotics*, 2(3), 96–106.

Katzschmann, R. K., Della Santina, C., Toshimitsu, Y., Bicchi, A., & Rus, D. (2019). Dynamic Motion Control of Multi-Segment Soft Robots Using Piecewise Constant Curvature Matched with an Augmented Rigid Body Model. In *2019 2nd IEEE International Conference on Soft Robotics (RoboSoft)*, 454–461.

Li, M., Kang, R., Branson, D. T., & Dai, J. S. (2018). Model-Free Control for Continuum Robots Based on an Adaptive Kalman Filter. *IEEE/ASME Transactions on Mechatronics*, 23(1), 286–297.

Mattioni, A., Wu, Y., Ramirez, H., Gorrec, Y. Le, & Macchelli, A. (2018). Modelling and control of a class of lumped beam with distributed control. *IFAC-PapersOnLine*, 51(3), 217–222.

Ortega, R., Spong, M. W., Gomez-Estern, F., & Blankenstein, G. (2002). Stabilization of a class of underactuated mechanical systems via interconnection and damping assignment. *IEEE Transactions on Automatic Control*, 47(8), 1218–1233.

Park, J., & Sandberg, I. W. (1991). Universal Approximation Using Radial-Basis-Function Networks. *Neural Computation*, 3(2), 246–257.

Renda, F., Boyer, F., Dias, J., & Seneviratne, L. (2018). Discrete Cosserat Approach for Multisection Soft Manipulator Dynamics. *IEEE Transactions on Robotics*, 34(6), 1518–1533.

Runciman, M., Darzi, A., & Mylonas, G. P. (2019). Soft Robotics in Minimally Invasive Surgery. *Soft Robotics*, 6(4), 423–443.

Suzumori, K. (1996). Elastic materials producing compliant robots. *Robotics and Autonomous Systems*, 18(1-2), 135–140.

Thuruthel, T. G., Ansari, Y., Falotico, E., & Laschi, C. (2018). Control Strategies for Soft Robotic Manipulators: A Survey. *Soft Robotics*, 5(2), 149–163.

Thuruthel, T. G., Falotico, E., Manti, M., Pratesi, A., Cianchetti, M., & Laschi, C. (2017). Learning Closed Loop Kinematic Controllers for Continuum Manipulators in Unstructured Environments. *Soft Robotics*, 4(3), 285–296.